Kinetic Explanation for the Temperature Dependence of the Regioselectivity in the Hydroformylation of Neohexene

Sabriye Güven,[a] Marko M. L. Nieuwenhuizen,[a] Bart Hamers,[b] Robert Franke,[b] Markus Priske,[b] Marc Becker,[b] and Dieter Vogt*[a, c]

The kinetics of Rh-catalyzed neohexene hydroformylation were investigated with the bulky monodentate ligand tris(2,4-di-*tert*-butylphenyl)phosphite. The hydrogenolysis of the Rh–acyl intermediate was identified as the rate-limiting step for both the linear and the branched aldehydes. Rate equations for both aldehydes were derived and kinetic parameters were estimated. Increased aldehyde linearity at higher temperatures, frequently observed in hydroformylation, was elucidated by deuterioformylation experiments. These showed that at 100 °C the formation of linear Rh–alkyl was more reversible than the formation of the branched derivative. The ratio of linear to branched Rh–acyl species was determined by in situ high-pressure IR spectroscopy experiments, which allowed the difference in the activation energies for the hydrogenolysis steps towards the aldehyde isomers to be quantified. The hydrogenolysis of Rh–acyl was found to be the step that caused the greatest temperature effect on the regioselectivity.

Introduction

The hydroformylation of alkenes, discovered in 1938 by Otto Roelen, has become one of the most important homogenously catalyzed reactions in industry and has been studied extensively.[1] Nowadays, rhodium is most commonly applied as the catalyst metal, and a great variety of phosphorus ligands are available to tune the catalyst for activity and selectivity. Knowledge about the influence of their steric and electronic properties usually allows good prediction of the expected activity and selectivity of the catalyst system. Bulky monodentate π-accepting ligands give rise to extremely active but less regioselective catalysts, whereas chelating ligands possessing a large bite angle allow for very high selectivity towards the linear aldehyde product.[2] However, knowledge of the catalyst itself is usually not enough for the prediction of reactivity; different elementary steps in the mechanism can become rate limiting for different
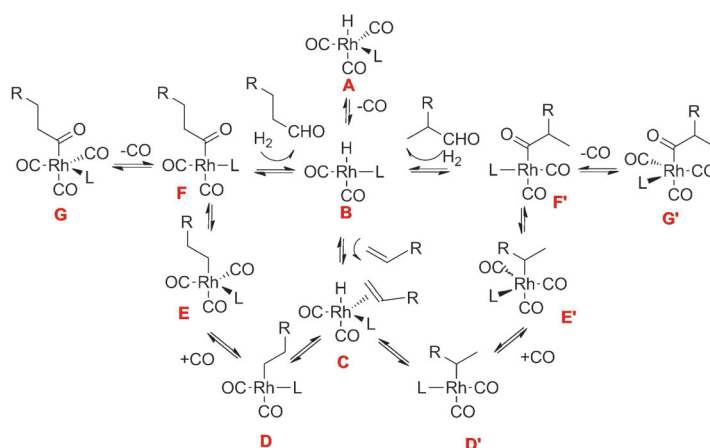
Scheme 1. Mechanism of Rh-catalyzed hydroformylation when using bulky monophosphites.[3]

substrates, even for isomers, depending on the position of the double bond in the molecule.[3,4]

Regioselectivity in Rh-catalyzed hydroformylation is a widely studied subject,[5–8] owing to its industrial relevance,[9] and the linear aldehyde is typically the desired product in large-scale applications.[1] In the literature, the formation of Rh–alkyl in the reaction mechanism (Scheme 1) is generally referred to as the step that determines the regioselectivity, especially at low temperatures, for which the formation of Rh–alkyl is not reversible.[5] At higher temperatures, the higher reversibility of the branched Rh–alkyl formation step has been shown to favor the linear product.[2,10,11] However, a detailed in situ kinetic study of the rate-limiting Rh–acyl hydrogenolysis step revealed a difference in energetics for the linear and branched isomers for styrene hydroformylation.[6] Finally, it is well reported that hydro-

[a] S. Güven, M. M. L. Nieuwenhuizen, Prof. Dr. D. Vogt
Faculteit Scheikundige Technologie
Technische Universiteit Eindhoven
P.O. Box 513, 5600 MB Eindhoven (The Netherlands)
Fax: (+ 44) 131-650-6453
E-mail: d.vogt@ed.ac.uk

[b] Dr. B. Hamers, Prof. Dr. R. Franke, Dr. M. Priske, Dr. M. Becker
Evonik Oxeno GmbH
Paul-Baumann-Str. 1, 45772 Marl (Germany)

[c] Prof. Dr. D. Vogt
School of Chemistry
University of Edinburgh
West Mains Road Edinburgh EH9 3JJ Scotland (United Kingdom)

Supporting information for this article is available on the WWW under http://dx.doi.org/10.1002/cctc.201300818.

formylation regioselectivity is governed by a combination of different steps in the mechanism and is dependent on reaction conditions, catalytic system, and substrate.[7,12]

For the design and operation of a jet-loop reactor with integrated membrane filtration for continuous homogeneously catalyzed hydroformylation, we needed accurate kinetic data for a number of model substrates, such as neohexene, and for a wider range of operating conditions.[13] While examining the kinetics of neohexene hydroformylation, we came across some inconsistencies that could not be explained by the common interpretation. Aroused by curiosity, we decided to perform an in-depth study.

The kinetics of neohexene hydroformylation (Scheme 2) were previously investigated for the tris(2-*tert*-butyl-4-methylphenyl)phosphite-modified rhodium catalyst.[14] Van Leeuwen et al. found a first-order dependence of the reaction rate on alkene concentration and hence proposed alkene coordination
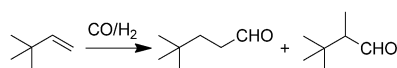
Scheme 2. Neohexene hydroformylation.

to be the rate-limiting step. Under the reaction conditions studied, they did not observe any branched product and concluded that the steric bulk of the substrate, which hampers its coordination, also prevents its coordination in the branched fashion.

Under the same conditions used for tris(2-*tert*-butyl-4-methylphenyl)phosphite,[14] Selent et al. observed the formation of 5% branched aldehyde in the product by using the bulky tris(2,4-di-*tert*-butylphenyl)phosphite rhodium catalyst.[15] Formation of both aldehydes followed pseudo-first-order kinetics, with an initial constant reaction rate followed by a first-order alkene dependence at higher conversions. In situ IR spectroscopy studies by the same authors confirmed the reformation of the Rh–hydride species together with the Rh–acyl species as observable intermediates during the reaction. According to this study, hydrogenolysis of the Rh–acyl species is the rate-limiting step over the entire conversion range. The authors observed an increase in the amount of branched aldehyde produced with decreasing temperature and proposed that this might be due to the difference in activation energies of hydrogenolysis steps of the isomeric aldehydes.

Aiming to elucidate the reasons behind the temperature dependence of the regioselectivity, we investigated the kinetics of neohexene hydroformylation for the tris(2,4-di-*tert*-butylphenyl)phosphite rhodium catalyst and performed deuterioformylation reactions and in situ IR spectroscopy measurements to quantify the contributions of different elementary steps in the mechanism to this behavior.

Results and Discussion

Kinetics

Neohexene hydroformylation produces two isomeric aldehydes, 4,4-dimethylpentanal and 2,3,3-trimethylbutanal, as shown in Scheme 2, which will be referred to as the linear (l) and branched (b) aldehydes, respectively.

Bulky phosphites are reported to result in monocoordinated active Rh species.[15–17] In this study, we used a high molar excess of the ligand (L/Rh varying from 15 to 30) to ensure the complete coordination of all Rh centers and to avoid observing mixed kinetics of ligated and unmodified Rh. A mechanistic study performed by van Leeuwen et al. reports that the IR spectra of the Rh–H species contained three carbonyl bands if an excess of L/Rh = 15 was applied, which points to the presence of monoligated species.[16] The hydroformylation mechanism proposed for the bulky phosphite monoligated Rh catalyst is given in Scheme 1.[3] According to this mechanism and the findings in the literature,[15] we derived the following rate (r) equations [Equations (1) and (2)] for linear and branched aldehydes by assuming that the hydrogenolysis step was rate limiting for both the linear and branched aldehydes (detailed derivation of the equations is given in the Supporting Information).

$$r_l = \frac{k_{FA}K_{AB}K_{BC}K_{CF}[\text{Rh}][\text{Alkene}][\text{H}_2]}{1 + K_{AB}K_{BC}(K_{CF}K_{FG} + K'_{CF}K'_{FG})[\text{Alkene}][\text{CO}]} \quad (1)$$

$$r_b = \frac{k'_{FA}K_{AB}K_{BC}K'_{CF}[\text{Rh}][\text{Alkene}][\text{H}_2]}{1 + K_{AB}K_{BC}(K_{CF}K_{FG} + K'_{CF}K'_{FG})[\text{Alkene}][\text{CO}]} \quad (2)$$

In the equations, k stands for the rate constant and K stands for the equilibrium constant of the step specified in the subscript (see Scheme 1 for reaction steps). It is possible to simplify these equations by lumping equilibrium constants together as given in Equations (3) and (4).

$$r_l = \frac{k_l[\text{Rh}][\text{Alkene}][\text{H}_2]}{1 + K[\text{Alkene}][\text{CO}]} \quad (3)$$

$$r_b = \frac{k_b[\text{Rh}][\text{Alkene}][\text{H}_2]}{1 + K[\text{Alkene}][\text{CO}]} \quad (4)$$

Parameters are k_l and k_b are Arrhenius-type rate constants with frequency factors A_l and A_b for the linear and branched aldehydes, respectively, and with activation energies ΔE_{Al} and ΔE_{Ab}.

Two reactions were performed: both at 80 °C, 20 bar CO, one at 20 bar H_2 and the other at 40 bar H_2 (1 bar = 100 kPa); to check the assumption that hydrogenolysis is the rate limiting step for both aldehydes. If any one of the aldehydes had a different rate-limiting step, the linear to branched aldehyde ratio (l/b ratio) would change. Both reactions gave the same linear/branched aldehyde ratio of 18.5. Moreover, monitoring the reaction profile by sampling during the reaction gave a similar profile for both aldehydes, as shown in Figure 1.

During this reaction, the l/b ratio was constant at approximately 23.2 ± 0.6. This behavior was confirmed at both 80 and
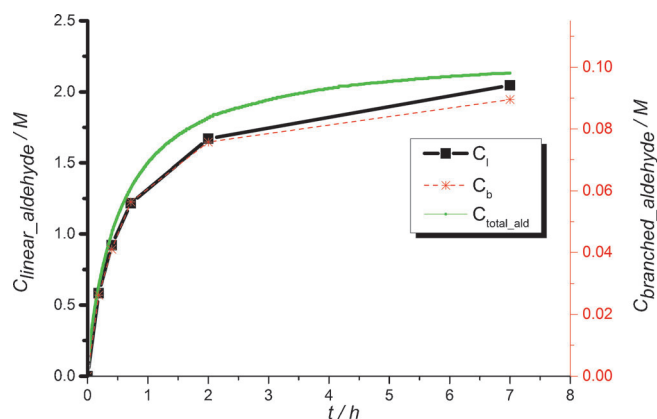
Figure 1. Sampling semibatch deuterioformylation reaction showing reaction profiles for both the linear and branched aldehydes and the total aldehyde profile obtained by the gas uptake curve. Reaction conditions: [neohexene] = 2.7 M, [Rh] = 1.0 × 10⁻⁴ M, L/Rh = 27, CO = 20 bar, D₂ = 20 bar, T = 100 °C.

50 °C, as given in the Supporting Information (Table S1). Both the experiment with double the hydrogen pressure and the sampling experiments confirmed that the hydrogenolysis step was the common rate-limiting step for both aldehydes.

Semibatch hydroformylation experiments were performed to determine the parameters in the rate equation—frequency factors, activation energies, and the lumped equilibrium constant K. Reaction variables appearing in the rate equation (Rh and alkene concentrations, H_2 and CO pressures, and reaction temperature) were varied, as given in the Supporting Information. The ligand concentration was also varied for some of the experiments to confirm that L/Rh = 15 was already a large enough excess of ligand and that increasing the L/Rh ratio would not affect the regioselectivity (Figure S1 shows l/b vs. L/Rh). H_2 and CO concentrations were kept constant by using a mass flow controller that fed syngas (CO/H_2 = 1:1) to keep the reaction pressure and the preadjusted CO/H_2 ratio constant. This approach enabled us to register the gas uptake values over time, which was easily correlated to alkene conversion, that is, total aldehyde concentration (as given in Figure 1), as the maximum amount of alkene hydrogenation observed in the study was 1.4% and the formation of alcohol or heavies, such as aldol condensation products, was not observed.

Concentration–time data for kinetic evaluation was obtained by using the gas uptake curves. Given that l/b was shown to be constant over the reaction range, the respective concentrations of the linear and branched aldehydes were calculated by using the l/b value determined at the end of the reaction time. Concentration values at 10, 30, 50, and 70% neohexene conversion were used together with the time data determined by using the "lookup" function of Microsoft Excel for the gas uptake data of each experiment (given in the Supporting Information). Nonlinear regression analysis of the kinetic data was performed by using a MATLAB routine developed according to the algorithm reported by Koeken et al.[18] This routine numerically integrates the batch design equations for neohexene and

linear and branched aldehydes given in Equations (5)–(7). We assumed that the concentrations of CO and H_2 were constant for these semibatch reactions, as we made sure to operate at non-mass-transfer limited conditions and we kept compensating both gases by keeping the reaction pressure constant. (Detailed explanation of how gas concentrations in solution were calculated is given in the Supporting Information.) To estimate these equations, the optimization routine uses updated guesses of the rate equation parameters mentioned for Equations (3) and (4) for each iteration by starting from user-supplied initial guesses. The optimizer compares the experimental concentration values to the concentration values estimated at times determined as explained before by solving the differential equations and keeps changing the parameter values until the difference between the estimated and experimental data converges to a minimum.

$$\frac{d[\text{neohexene}]}{dt} = -r_l - r_b \tag{5}$$

$$\frac{d[\text{linear\_aldehyde}]}{dt} = r_l \tag{6}$$

$$\frac{d[\text{branched\_aldehyde}]}{dt} = r_b \tag{7}$$

Optimal parameter values are presented in Table 1 with their 95% confidence intervals. Figure 2 compares experimental concentration data from the kinetic experiments and data estimated by using the parameter values presented in Table 1. Es-

Table 1. Parameter values for rate equations of linear and branched aldehydes [Equations (3) and (4)].

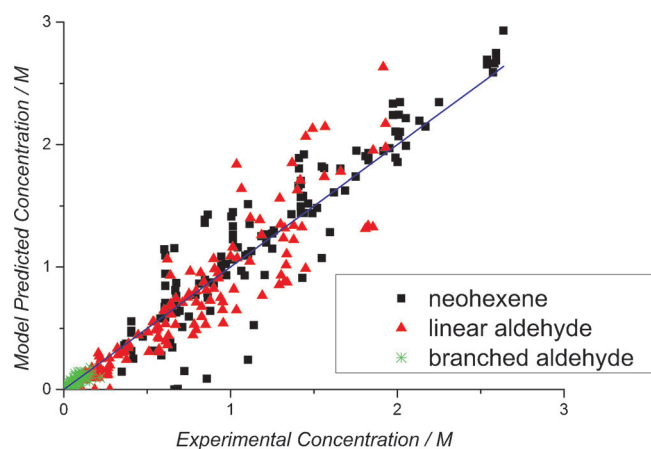| Parameter	Value
A_l [M⁻² min⁻¹]	$(1.45 \pm 0.66) \times 10^{17}$
ΔE_{Al} [kJ mol⁻¹]	85.54 ± 1.86
A_b [M⁻² min⁻¹]	$(5.83 \pm 0.90) \times 10^{11}$
ΔE_{Ab} [kJ mol⁻¹]	56.87 ± 0.31
K [M⁻²]	40.00 ± 1.05

Figure 2. Parity plot comparing estimated and experimental concentration data from the semibatch experiments.

timated data are in good agreement with the experimental data.

Regioselectivity

Given that the l/b ratio was shown to be constant during the reaction, it was possible to model the regioselectivity as given in Equation (8) by using the parameter values given in Table 1.

$$\frac{l}{b} = \frac{r_l}{r_b} = \frac{A_l \exp\left(-\Delta E_{Al}/RT\right)}{A_b \exp\left(-\Delta E_{Ab}/RT\right)} = \frac{A_l}{A_b} \exp\left(\frac{-\Delta E_{Al} + \Delta E_{Ab}}{RT}\right) \quad (8)$$

Equation (8) suggests that the regioselectivity is a function of temperature only. Figure 3 shows the percentage of linear aldehyde in the product depending on the reaction tempera-
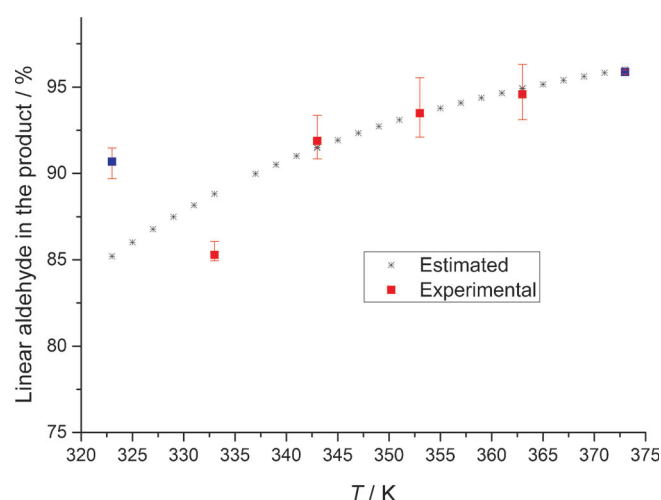

Figure 3. Percentage of linear aldehyde in the product as a function of temperature; values were obtained from kinetic hydroformylation experiments and estimated by Equation (8). Data points at 323 and 373 K belong to deuterioformylation experiments.

ture, obtained from the semibatch hydroformylation reactions performed for the kinetics and estimated by using Equation (8). There is a clear increase in the percentage of linear aldehyde in the product with increasing temperature, especially evident in the lower temperature region. The model predicts the higher temperature region, for which more experimental data was available, better than the lower temperature region. Specifically, the data points for 50 °C, measured for deuterioformylation experiments, are quite higher than the predicted values. Further experiments in the lower temperature region are required to clear this point.

This behavior can be the result of a shift in the equilibrium for Rh–alkyl formation with increasing temperature that favors the formation of linear Rh–alkyl.[19] Another reason can be a difference in the activation energies of the hydrogenolysis steps. If the activation energy for the formation of the linear aldehyde was higher than that for the branched isomer, the rate

constant for the formation of the linear aldehyde should have a stronger temperature dependence.[15]

For the sake of simplicity, we have lumped together the equilibrium and rate constants in Equations (1) and (2) and expressed them in the form of Arrhenius dependency. Writing them in their original forms as in Equation (9) will help to show the role of these two probable sources of temperature effects on the regioselectivity.

$$\frac{r_l}{r_b} = \frac{k_{FA} K_{CF}}{k'_{FA} K'_{CF}} = \frac{A_{FA} \exp\left(-\Delta E_{FA}/RT\right) \exp\left(-\Delta G_{CF}/RT\right)}{A'_{FA} \exp\left(-\Delta E'_{FA}/RT\right) \exp\left(-\Delta G'_{CF}/RT\right)} \quad (9)$$

Lumped activation energies ΔE_{Al} and ΔE_{Ab}, which represent the whole cycle for linear and branched aldehydes, differ by 28.7 kJ mol^{-1}, as shown in Equation (8). This difference is a combination of the differences in activation the energies (ΔE_{FA} and $\Delta E'_{FA}$) for the hydrogenolysis step and the Gibbs free energies of the equilibrium steps (ΔG_{CF} and $\Delta G'_{CF}$) between the π complex (species **C** and **C′**) and Rh–acyl (species **F** and **F′**). To quantify these effects, deuterioformylation and in situ IR spectroscopy experiments were performed.

Deuterioformylation experiments

Hydroformylation experiments performed under D$_2$ pressure instead of H$_2$ give direct information on the reversibility of the Rh–alkyl formation step (**C** to **D**).[10, 20] The use of the Rh catalyst under D$_2$ pressure will label the alkene reversed from branched Rh–alkyl at C1, whereas it will label the alkene reversed from linear Rh–alkyl at C2, as shown in Scheme 3.
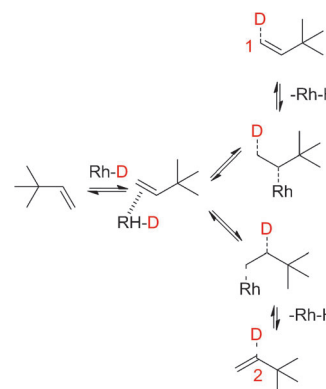
Scheme 3. Deuterium labeling of alkene molecules reversed from Rh–alkyl formation under deuterioformylation conditions.

Three deuterioformylation reactions were performed with D$_2$/CO (20:20 bar) at 50, 80, and 100 °C to investigate the effect of temperature on Rh–alkyl reversibility. A fourth experiment was performed at 50 °C and 20:10 bar D$_2$/CO to check if CO pressure had any effect on the reversibility of the Rh–alkyl species. There might be a different effect on the equilibrium following linear Rh–alkyl formation (**D** to **E**) compared to the branched one (**D′** to **E′**).[21] If one of these equilibria is more

sensitive to the CO concentration, this would shift the rate-limiting step to CO insertion into the Rh–alkyl species (**D** to **E**) at lower CO concentrations. However, care should be taken to prevent CO depletion, that is, not to work under gas–liquid mass-transfer control. Deuterium incorporations into the C1 (terminal) and C2 (internal) positions were determined by analysis of samples taken during the course of the reactions by ^{2}H NMR spectroscopy. As seen from Figure 4, the fraction of
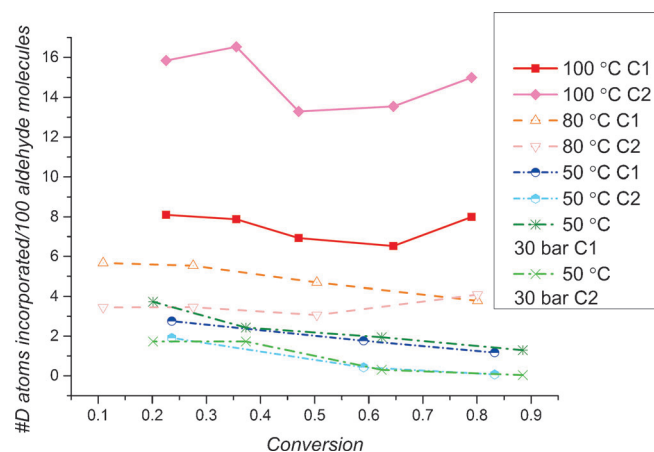

Figure 4. Deuterium incorporation into the C1 (terminal) and C2 (internal) positions of neohexene during deuterioformylation: [neohexene] = 2.7 м, [Rh] = 1.0 × 10⁻⁴ м, L/Rh = 27, CO = 20 bar unless otherwise stated, D₂ = 20 bar.

deuterium atoms incorporated with respect to the number of aldehyde molecules produced increased with increasing temperature for both positions.

An important observation is that at 100 °C the number of D atoms on C2 was higher than that on C1. Hence, the equilibrium for linear Rh–alkyl formation is more temperature sensitive than the equilibrium for branched Rh–alkyl formation. This behavior is easily observed in Figure 5, for which the fraction of D atoms in the C1 and C2 positions averaged over the entire conversion range is plotted.
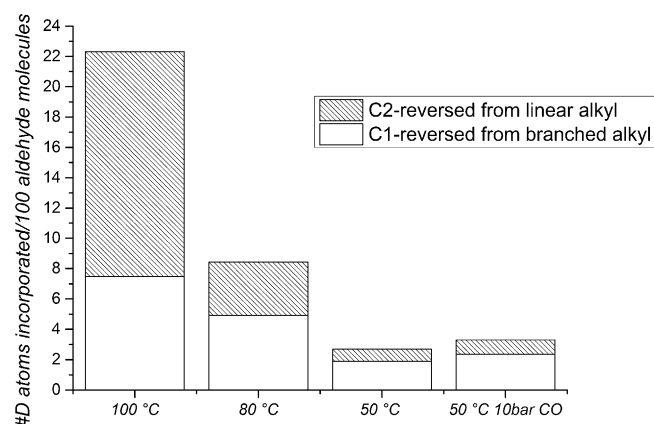

Figure 5. Average deuterium incorporation into the C1 (terminal) and C2 (internal) positions of neohexene during deuterioformylation for conditions given in Figure 3.

The temperature sensitivity of an equilibrium arises from the entropy change associated with this step. Given $\Delta G = \Delta H - T\Delta S$, the entropy term will affect the equilibrium more at higher temperatures. Rh–alkyl formation should have a negative entropy change, as one molecule is formed from two molecules and a negative change in entropy will favor the reverse reaction, even more so at increased temperature. Thus, the increase in reversed linear Rh–alkyl with temperature suggests that the negative change in entropy for linear Rh–alkyl formation is higher than the negative change in entropy for branched Rh–alkyl formation and consequently that linear Rh–alkyl has lower entropy. Reducing the CO pressure did not have an effect on the reversibility at 50 °C. This is an expected result and confirms that hydrogenolysis is the common rate-limiting step.

High-pressure IR experiments

Although deuterioformylation experiments give a clear idea of the reversibility for the linear and branched Rh–alkyl species, they do not help to quantify the activation energy difference in the hydrogenolysis step. Only an analysis of the respective amounts of the Rh–acyl species would give direct information on that,[6] as explained in the derivation of Equations (10) and (11).

$$\frac{d\mathbf{C}_{\text{l\_aldehyde}}}{dt} = k_{\text{FA}}[\mathbf{F}][H_2] \tag{10}$$

$$\frac{d\mathbf{C}_{\text{l\_aldehyde}}}{dt} = \frac{k_{\text{FA}}[\mathbf{G}][H_2]}{K_{\text{FG}}[\text{CO}]} \tag{11}$$

According to the justified assumption that l/b is constant during the reaction, it is possible to write Equation (12), and by comparing Equation (12) to Equation (9), Equation (13) can be written as given.

$$\frac{d\mathbf{C}_{\text{l\_aldehyde}}}{d\mathbf{C}_{\text{b\_aldehyde}}} = \frac{\text{l}}{\text{b}} = \frac{k_{\text{FA}}K'_{\text{FG}}[\mathbf{G}]}{k'_{\text{FA}}K_{\text{FG}}[\mathbf{G}']} = \frac{A_{\text{FA}}\exp\left(-\Delta E_{\text{FA}}/RT\right)K'_{\text{FG}}[\mathbf{G}]}{A'_{\text{FA}}\exp\left(-\Delta E'_{\text{FA}}/RT\right)K_{\text{FG}}[\mathbf{G}']}$$

$$\frac{\text{l}[\mathbf{G}']}{\text{b}[\mathbf{G}]} = \frac{A_{\text{FA}}\exp\left(\frac{-\Delta E_{\text{FA}}}{RT}\right)\exp\left(\frac{\Delta S'_{\text{FG}}-\Delta S_{\text{FG}}}{R}\right)\exp\left(\frac{\Delta H'_{\text{FG}}-\Delta H_{\text{FG}}}{RT}\right)}{A'_{\text{FA}}\exp\left(\frac{-\Delta E'_{\text{FA}}}{RT}\right)} \tag{12}$$

$$\frac{[\mathbf{G}]}{[\mathbf{G}']} = \frac{K_{\text{FG}}\exp\left(-\Delta G_{\text{CF}}/RT\right)}{K'_{\text{FG}}\exp\left(-\Delta G'_{\text{CF}}/RT\right)} = \frac{\exp\left(-\Delta G_{\text{CF}}/RT\right)\exp\left(-\Delta G_{\text{FG}}/RT\right)}{\exp\left(-\Delta G'_{\text{CF}}/RT\right)\exp\left(-\Delta G'_{\text{FG}}/RT\right)}$$

$$= \exp\left(\frac{\Delta S_{\text{CG}}-\Delta S'_{\text{CG}}}{R}\right)\exp\left(\frac{-\Delta H_{\text{CG}}+\Delta H'_{\text{CG}}}{RT}\right) \tag{13}$$

The ratio of the pre-exponential factors $A_{\text{FA}}/A'_{\text{FA}}$ enables us to calculate the difference in activation entropy changes, as given in Equation (14).

$$\frac{A_{FA}}{A'_{FA}} = \exp\left(\frac{\Delta S_{FA} - \Delta S'_{FA}}{R}\right) \tag{14}$$

The ratio of linear to branched Rh–acyl [**G**]/[**G′**] also provides direct information on the Gibbs free-energy differences of the steps between species **C** and **G**, as given in Equation (13). In situ IR spectroscopy experiments were performed to quantify the respective amounts of linear and branched Rh–acyl species. Figure 6 shows the spectra recorded in the first 10 min of the reaction performed at room temperature.
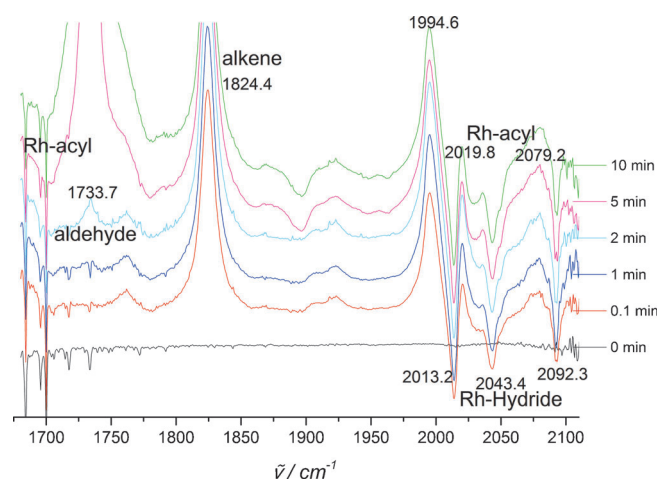

Figure 6. IR spectra recorded in the first 10 min of neohexene hydroformylation, [neohexene] = 0.54 M, [Rh] = 3.14×10⁻⁴ M, L/Rh = 26, T = 25 °C.

Negative bands appearing after the addition of neohexene ($\tilde{v}$ = 1824.4 cm⁻¹) belong to hydride species **A**, characterized by bands at 2013, 2043, and 2092 cm⁻¹. These values are in close agreement with the ones reported in the literature ($\tilde{v}_{CO}$ = 2013, 2041, and 2091 cm⁻¹).[15] They are negative because the background was measured after complete conversion of the catalyst into the Rh–hydride species, and after substrate addition some of this species turned into Rh–acyl. The Rh–acyl species (i.e., **G**, **G′**) is characterized by three bands in the terminal CO region: $\tilde{v}$ = 1994.6, 2019.8, and 2078 cm⁻¹, which appeared immediately after the addition of the substrate, also in agreement with the reported values[15] ($\tilde{v}_{CO}$ = 1995, 2017, 2079 cm⁻¹).

The bands belonging to the acyl C=O bond should appear in the organic carbonyl region[22,23] at approximately 1690–1700 cm⁻¹. These enabled us to determine the ratio of linear and branched Rh–acyl. This band was recently reported to appear at 1690 cm⁻¹ for this catalyst–substrate system.[17] However, the aldehyde (1734 cm⁻¹) and neohexene (1642 cm⁻¹) bands overlap in this region, and it was not possible to observe the relatively small C=O bands, especially at higher conversions. Therefore, the spectra of pure neohexene were subtracted from the recorded reaction spectra. The neohexene signal at 1824.4 cm⁻¹ was used to determine the proper amount of neohexene to be subtracted; spectra of different amounts of neohexene were subtracted and the one that eliminated the band at this position was chosen. The low pressure

Table 2. Ratio of linear to branched Rh–acyl species and reaction conditions for the IR spectroscopy experiments.

T [K]	H₂[a]	CO[a]	[G]/[G′]
298	4.85	35.15	1.04
313	3.87	34.21	1.12
328	6.59	29.75	1.50
343	3.75	31.00	1.68

[a] In units of bar at 25 °C (1 bar = 100 kPa).

of hydrogen used in these experiments (Table 2) enabled us to take a number of spectra before the Rh–acyl band was concealed under the aldehyde band at 1734 cm⁻¹. In this way, we were able to obtain the spectra of the acyl C=O bond of the Rh–acyl species as given in Figure 7, with desired species **G** and **G′** overlapping at approximately 1690 cm⁻¹.
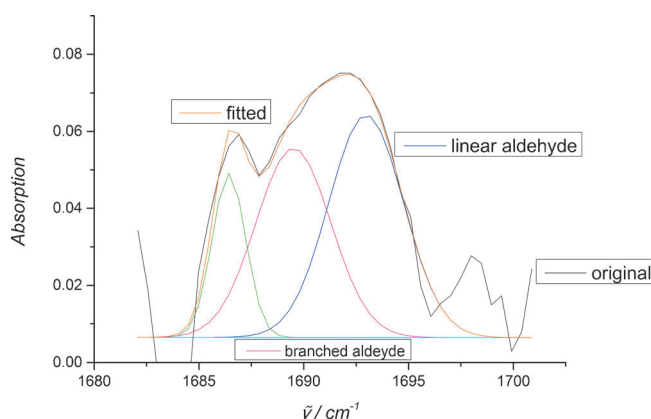

Figure 7. IR spectra recorded 8 min after neohexene addition for the 40 °C IR spectroscopy experiment after neohexene subtraction, showing the deconvolution of the Rh–acyl species.

After deconvolution of this band, linear and branched coordinatively saturated Rh–acyl species **G** and **G′** were characterized by the bands at 1693 and 1689.5 cm⁻¹, respectively, with the values given in Table 2. The deconvolutions were performed by CasaXPS,[24] and the final values were obtained by averaging the acyl ratios calculated from a number of spectra for each temperature. (More data on deconvolutions are available in the Supporting Information)

Rearranging Equation (13), the natural logarithm of the Rh–acyl ratios ln([**G**]/[**G′**]) describes a line as given in by Equation (15).

$$\ln\left(\frac{[G]}{[G']}\right) = \left(\frac{-\Delta H_{CG} + \Delta H'_{CG}}{RT}\right) + \left(\frac{\Delta S_{CG} - \Delta S'_{CG}}{R}\right) \tag{15}$$

Linear regression with data given in Table 2 allowed $\Delta H_{CG} - \Delta H'_{CG}$ to be calculated as 9.7 kJ mol⁻¹ and a difference of changes in entropy $\Delta S_{CG} - \Delta S'_{CG}$ as 32.5 J mol⁻¹ K⁻¹ (a figure showing the linear fit is given in Figure S2). It would be justified to assume that the total change in free energy from species **C** to **F** is negative, because the coordination of an alkene

is commonly thought to be a high-energy change step, as evidenced by the energy profiles of hydroformylation for a range of substrates.[8,21,22,25] The change in free energy of the equilibrium between **F** and **G** should also be negative. We also know that the difference in Gibbs free-energy changes is negative ($\Delta G_{CG} - \Delta G'_{CG} < 0$), from which we can deduce $|\Delta G_{CG}| > |\Delta G'_{CG}|$. So, a higher negative value of ΔG favors the forward reaction (**C** to **G**) of the linear path, even more so with increasing temperature, because the entropy difference $\Delta S_{CG} - \Delta S'_{CG}$ is positive and increases the difference in Gibbs free-energy changes with increasing temperature; as should be evident from the expression given in Equation (16).

$$\Delta G_{CG} - \Delta G'_{CG} = \Delta H_{CG} - \Delta H'_{CG} - T(\Delta S_{CG} - \Delta S'_{CG}) \tag{16}$$

It is now possible to obtain the values of the expressions given in Equations (17) and (18) by using the data in Table 2 for linear regression of Equation (12). (Figure showing the linear fit is given in Figure S3.)

$$(\Delta E_{FA} - \Delta H_{FG}) - (\Delta E'_{FA} - \Delta H'_{FG}) \tag{17}$$

$$\Delta S_{FA} - \Delta S'_{FA} - \Delta S_{FG} + \Delta S'_{FG} \tag{18}$$

Thus, $(\Delta E_{FA} + \Delta H_{GF}) - (\Delta E'_{FA} + \Delta H'_{GF}) = \Delta H_{GA} - \Delta H'_{GA} = 19 \text{ kJ mol}^{-1}$ and $\Delta S_{FA} - \Delta S'_{FA} + \Delta S_{GF} - \Delta S'_{GF} = \Delta S_{GA} - \Delta S'_{GA} = 71 \text{ J mol}^{-1} \text{K}$. For the formation of the activated state of the hydrogenolysis step, the entropy change should be positive. Garland et al.[26] reported an activation entropy of $\Delta S^{\#} = (121 \pm 14) \text{ J mol}^{-1} \text{K}^{-1}$ for the hydrogenolysis step in neohexene hydroformylation catalyzed by an unmodified Rh catalyst. A positive value for the activation entropy suggests that the transition state is highly unstable. Degrees of freedom are "liberated" in going from the ground state to the transition state, which, in turn, increase the rate of the reaction. The entropy change involved in going from **G** to **F** or from **G′** to **F′** should also be positive, and consequently, both ΔS_{GA} and $\Delta S'_{GA}$ are positive.

So, hydrogenolysis of five-coordinated linear Rh–acyl **G** under typical hydroformylation conditions is faster than that of branched isomer **G′** although it has a higher activation energy ($\Delta H_{GA} - \Delta H'_{GA} = 19 \text{ kJ mol}^{-1}$) because it has a larger positive activation entropy ($\Delta S_{GA} - \Delta S'_{GA} = 71 \text{ J mol}^{-1} \text{K}^{-1}$).

In summary, the part of the reaction cycle from species **C** to **G** has a higher enthalpy change than the equivalent part in the branched cycle, $\Delta H_{CG} - \Delta H'_{CG} = 9.7 \text{ kJ mol}^{-1}$. The hydrogenolysis of linear acyl **G** creates an enthalpy change that is 19 kJ mol^{-1} more than the change involved in the hydrogenolysis of branched acyl **G′**, $\Delta H_{GA} - \Delta H'_{GA} = 19 \text{ kJ mol}^{-1}$. The sum of these two figures determines the temperature sensitivity of the l/b ratio; this adds up to 28.7 kJ mol^{-1}, which was found as the difference between the lumped activation energies for linear and branched aldehydes, $\Delta E_{Al} - \Delta E_{Ab}$, as given in Equation (8). The difference in the parts of the reaction cycle from **G** to **A** and from **G′** to **A′** has a higher contribution to the temperature dependence of regioselectivity.

Conclusions

Detailed analysis of the kinetics and mechanism of Rh-catalyzed neohexene hydroformylation was performed for the tris(2,4-di-*tert*-butylphenyl)phosphite ligand. The rate-limiting step for both the linear and branched aldehydes was shown to be the hydrogenolysis of the Rh–acyl species. Rate equations were derived, and equation parameters were estimated within very narrow confidence intervals by using nonlinear regression. These estimates were used to predict the regioselectivity, which was in good agreement with the experimental data. Deuterioformylation and in situ IR spectroscopy experiments were performed to reveal the reasons behind the increase in linear aldehyde selectivity with increasing temperature.

The deuterioformylation experiments showed that the formation of both the linear and branched Rh–alkyl species was reversible and that the reverse reaction was favored at higher temperatures. This finding suggested that the entropy change involved in Rh–alkyl formation was negative. At 100 °C, linear Rh–alkyl formation was more reversible than branched Rh–alkyl formation, which implies the negative entropy change for linear Rh–alkyl formation is larger than that for branched Rh–alkyl formation: that is, the equilibrium for linear Rh–alkyl formation (**C** to **D**) is more temperature sensitive than the equilibrium for branched Rh–alkyl (**C** to **D′**). High-pressure IR spectroscopy experiments performed to investigate the linear and branched Rh–acyl species (**G** and **G′**) showed an excess amount of the linear Rh–acyl species relative to that of the branched species. Moreover, the ratio of linear to branched Rh–acyl increased with increasing temperature. These findings suggest that the total forward reaction of non-common equilibrium steps of the linear and branched catalytic cycles (**C** to **G** and **C** to **G′**) are favored for the linear aldehyde over the branched aldehyde.

Furthermore, the reverse step of the equilibrium from **G** to **F** and subsequent hydrogenolysis of linear acyl **F** was found to have a larger enthalpy change than the branched equivalent (**G′** to **F′** and hydrogenolysis of **F′**). The contribution of this part of the cycle to the temperature dependence of regioselectivity was approximately twice that from species **C** to **G** (and **C** to **G′**). Finally, the larger positive entropy changes for both mentioned parts of the linear aldehyde cycle make the linear aldehyde the favored isomer under typical hydroformylation conditions.

Experimental Section

Semibatch reactions for kinetics were performed in custom-built stainless steel autoclaves (100 mL) equipped with a mechanical gas-impeller stirrer. H_2 and CO concentrations were kept constant by using a mass flow controller that fed syngas (Linde Gas CO/H_2 = 1:1, ≥ 99.998 vol%) to keep the reaction pressure and the preadjusted CO/H_2 ratio constant. Reaction temperature was monitored during the reaction and was constant at the set temperature with a maximum of 2 °C overshoot in the first minutes. A total reaction volume of 10 mL (neohexene and toluene) was used for the kinetic experiments and the maximum amount of neohexene used was 5.5 mL. A stirring rate of 1200 rpm was set for all kinetic experi-

ments. Conversion was measured by gas chromatography (GC) by using an Agilent DB1 column (30 m×0.32 mm i.d.) at the end of the reaction time to confirm the values obtained from gas uptake (GU) data. The conversion values were generally in good agreement, with $x_{GC}/x_{GU} = 1 \pm 0.05$. If $x_{GC}/x_{GU} < 1$, the difference can be attributed to leaking gas or an overshoot in the measurement of the amount of neohexene by using a graduated syringe. For $x_{GC}/x_{GU} > 1$, the initial amount of neohexene can also be lower as a result of experimental error or loss of neohexene while charging the volatile neohexene to the autoclave under Ar atmosphere. For the sake of consistency, the amount of neohexene charged into the autoclave was recalculated according to the GU value at full conversion for all cases. All solutions were prepared under an atmosphere of argon by using Schlenk techniques. The substrate solution containing neohexene (Sigma–Aldrich, $\geq 97\%$) and decane (Sigma–Aldrich, $\geq 99\%$) as an internal standard was filtered over neutral alumina and degassed. A stock solution of the catalyst [Rh(acac)(CO)$_2$, acac = acetylacetonate, obtained as a generous loan from OMG] and ligand [tris(2,4-di-tert-butylphenyl)phosphite, Sigma–Aldrich, 98%] was prepared in dry and degassed toluene (purchased from Biosolve and purified over custom made alumina columns).

The substrate solution was brought into an addition funnel connected to the autoclave by a tube that kept the funnel at the same pressure as the autoclave and a valve that enabled controlled charge of the substrate solution into the autoclave. The catalyst solution was charged into the autoclave, and it was preformed under reaction conditions for 1 h, after which the reaction was started by adding the substrate solution. Complete conversion of the catalyst precursor into the Rh–H species was confirmed to occur in 40 min at 50 °C, which implies the preformation was complete for all the experiments in this study. (IR spectra of the preformation is given in Figure S4.)

Deuterioformylation reactions were performed with the same type of autoclave as mentioned above equipped with a sampling unit that enabled sampling during the reaction. The total reaction volume was 30 mL and the neohexene volume was 15 mL.

^{2}H NMR spectroscopy was performed with a Varian Unity Inova 500 spectrometer operating at 499.8 MHz for ^{1}H (76.72 MHz for ^{2}H), equipped with a 5 mm AutoX DB-PFG probe. Prior to measurement, the 90° pulse width was calibrated by using a solution of C$_6$D$_6$ in CHCl$_3$. Spectra were recorded by using a 1535 Hz spectral width by employing 90° pulses and a relaxation delay of 20 s. Data was processed by using VNMRJ 2.2d software and was filtered by using 1 Hz line broadening. Integrals were normalized to the aldehyde signal at 10.1 ppm

In situ high-pressure IR spectroscopy experiments were performed in a custom-built stainless steel autoclave (50 mL) with an integrated flow cell equipped with a ZnS windows and a mechanical gas-impeller stirrer (800 rpm for all FTIR measurements). The spectra were recorded with a Shimadzu FTIR 8300 spectrometer in the absorbance mode. A solution of the catalyst in hexane was preformed under an atmosphere of syngas, and the reaction was started after complete hydride formation by adding the substrate, which was kept in a dropping funnel. Background measurements were performed just before the addition of the substrate. FTIR spectra of pure neohexene were later subtracted from the measurements in proper amounts. Catalyst and substrate concentrations were kept constant at [neohexene] = 0.54 M, [Rh] = 3.14×10^{-4} M, and L/Rh = 26 for all experiments (total reaction volume 10 mL).

[1] P. W. N. M. van Leeuwen, C. Claver, *Rhodium Catalyzed Hydroformylation*, Springer, **2002**.
[2] S. C. van der Slot, J. Duran, J. Luten, P. C. J. Kamer, P. W. N. M. van Leeuwen, *Organometallics* **2002**, *21*, 3873–3883.
[3] A. van Rooy, E. N. Orij, P. C. J. Kamer, P. W. N. M. van Leeuwen, *Organometallics* **1995**, *14*, 34–43.
[4] B. Breit, W. Seiche, *Synthesis* **2001**, *2001*, 0001–0036.
[5] G. Alagona, C. Ghio, R. Lazzaroni, R. Settambolo, *Organometallics* **2001**, *20*, 5394–5404.
[6] J. Feng, M. Garland, *Organometallics* **1999**, *18*, 417–427.
[7] A. L. Watkins, C. R. Landis, *J. Am. Chem. Soc.* **2010**, *132*, 10306–10317.
[8] R. Lazzaroni, R. Settambolo, G. Alagona, C. Ghio, *Coord. Chem. Rev.* **2010**, *254*, 696–706.
[9] K.-D. Wiese, D. Obst in *Catal. Carbonylation React.* (Ed.: M. Beller), Springer, Berlin, **2006**, pp. 1–33.
[10] R. Lazzaroni, G. Uccello-Barretta, M. Benetti, *Organometallics* **1989**, *8*, 2323–2327.
[11] R. Lazzaroni, R. Settambolo, G. Uccello-Barretta, A. Caiazzo, S. Scamuzzi, *J. Mol. Catal. A* **1999**, *143*, 123–130.
[12] C. P. Casey, S. C. Martins, M. A. Fagan, *J. Am. Chem. Soc.* **2004**, *126*, 5585–5592.
[13] S. Güven, B. Hamers, R. Franke, M. Priske, M. Becker, D. Vogt, *Cat. Sci. Technol.* **2014**, DOI: 10.1039/C3CY00676J..
[14] A. Van Rooy, J. N. H. de Bruijn, K. F. Roobeek, P. C. J. Kamer, P. W. N. Van Leeuwen, *J. Organomet. Chem.* **1996**, *507*, 69–73.
[15] C. Kubis, R. Ludwig, M. Sawall, K. Neymeyr, A. Börner, K.-D. Wiese, D. Hess, R. Franke, D. Selent, *ChemCatChem* **2010**, *2*, 287–295.
[16] T. Jongsma, G. Challa, P. W. N. van Leeuwen, *J. Organomet. Chem.* **1991**, *421*, 121–128.
[17] C. Kubis, D. Selent, M. Sawall, R. Ludwig, K. Neymeyr, W. Baumann, R. Franke, A. Börner, *Chem. Eur. J.* **2012**, *18*, 8780–8794.
[18] A. C. J. Koeken, L. J. P. van den Broeke, B.-J. Deelman, J. T. F. Keurentjes, *J. Mol. Catal. A* **2011**, *346*, 1–11.
[19] R. Lazzaroni, P. Pertici, S. Bertozzi, G. Fabrizi, *J. Mol. Catal.* **1990**, *58*, 75–85.
[20] C. P. Casey, L. M. Petrovich, *J. Am. Chem. Soc.* **1995**, *117*, 6007–6014.
[21] C. Ghio, R. Lazzaroni, G. Alagona, *Eur. J. Inorg. Chem.* **2009**, 98–103.
[22] G. Liu, R. Volken, M. Garland, *Organometallics* **1999**, *18*, 3429–3436.
[23] P. C. J. Kamer, A. van Rooy, G. C. Schoemaker, P. W. N. M. van Leeuwen, *Coord. Chem. Rev.* **2004**, *248*, 2409–2424.
[24] http://www.casaxps.com/.
[25] G. Alagona, R. Lazzaroni, C. Ghio, *J. Mol. Model.* **2011**, *17*, 2275–2284.
[26] M. Garland, P. Pino, *Organometallics* **1991**, *10*, 1693–1704.
[27] J. H. Hildebrand, *Solubility of Non-electrolytes*, Reinhold Pub. Corp., **1936**.
[28] U. J. Jáuregui-Haza, E. J. Pardillo-Fontdevila, A. M. Wilhelm, H. Delmas, *Lat. Am. Appl. Res.* **2004**, *34*, 71–74.
[29] L. C. Yen, J. J. McKetta, *AIChE J.* **1962**, *8*, 501–507.